s-process branchings at ^{151}Sm, ^{154}Eu, and ^{163}Dy

J. Best, H. Stoll, C. Arlandini, S. Jaag, F. Käppeler, and K. Wisshak

Forschungszentrum Karlsruhe, Institut für Kernphysik, Postfach 3640, D-76021 Karlsruhe, Germany

A. Mengoni and G. Reffo

ENEA, Applied Physics Division, V. Don Fiammelli 2, I-40129 Bologna, Italy
and Centro Dati Nucleari, V. Martiri di Monte Sole 4, I-40129 Bologna, Italy

T. Rauscher

Institut für Physik, Universität Basel, Klingelbergstrasse 82, CH-4056 Basel, Switzerland

The (n,γ) cross sections of the stable europium isotopes ^{151}Eu and ^{153}Eu have been measured by irradiating oxide samples in a quasistellar neutron spectrum. From the induced activities, the stellar cross sections of ^{151}Eu and ^{153}Eu at a thermal energy of $kT=30$ keV were found to be $\langle \sigma v \rangle / v_T = 3821 \pm 152$ mb and 2733 ± 110 mb, respectively. These results allowed us to resolve severe discrepancies among previous data. Similar activation measurements were also performed on ^{152,154}Sm and ^{164,170}Er. Among these results, the stellar cross section of the s-only isotope ^{164}Er $\langle \sigma v \rangle / v_T = 1084 \pm 51$ mb at $kT=30$ keV is particularly important. Statistical model calculations were performed with emphasis on the effect of excited states as well as on the unstable isotopes ^{151}Sm, ^{152}Eu, and ^{154}Eu. The combined set of cross sections was used for an updated analysis of the branchings at $A=151$, 152, 154, and 163. The temperature and density estimates derived via the classical approach are discussed and compared to stellar models for helium shell burning in low mass stars.

I. INTRODUCTION

The mass region of the rare earth elements (REEs) from lanthanum to lutetium is of special importance for s-process studies for the following reasons.

(i) Since the REEs are chemically almost identical, their relative abundances are known to better than 2% [1]. Accordingly, the comparison of the s-process yields obtained by model calculations with the observed abundances of the s-only isotopes can be made at a confidence level that is comparable with the obtainable cross section uncertainties.

(ii) The REEs comprise isotopes with very different stellar (n,γ) cross sections ranging from the 11 mb of the neutron magic nucleus ^{140}Ce to values around 3000 mb observed for the odd-odd europium isotopes. This means that the abundances of the lightest REE can be used to probe the s-process reaction flow with respect to the bottle neck effect of the small cross sections at magic neutron number $N=82$, which has recently been noticed to constrain the s process in thermally pulsing stars on the asymptotic giant branch (AGB) [2].

On the other hand, the majority of the REE isotopes exhibit sufficiently large cross sections to satisfy the local approximation $N_s \langle \sigma \rangle = $ const, which implies that equilibrium had been established in the s-process reaction flow. In this case, the s abundances can be described by the schematic *classical approach* independently from particular s-process models.

(iii) The REE region includes a number of branchings in the s-process path. From the analysis of the respective abundance patterns, the main parameters—neutron density n_n, temperature T_s, and mass density ρ_s—characterizing the physical conditions during the s process can be derived. The determination of these parameters is greatly facilitated by the

well defined relative abundances of the REE as well as by the validity of the local approximation. In particular, this second aspect is important since it allows consistent studies of these branchings within the classical approach. In turn, these branchings constitute important tests for various aspects of stellar s-process models.

Figure 1 illustrates the s-process reaction flow in the investigated mass region with the major branchings at ^{151}Sm and ^{154}Eu which are defined by the s-only nuclei ^{152}Gd and ^{154}Gd, respectively. While these two nuclei are partly bypassed in the s process, the total reaction flow is represented by the neighboring s isotope ^{150}Sm. Both branchings can be considered as s-process thermometers since the competition between neutron capture and β decay is affected at stellar temperatures by the thermal population of low-lying excited states with shorter β lifetimes.

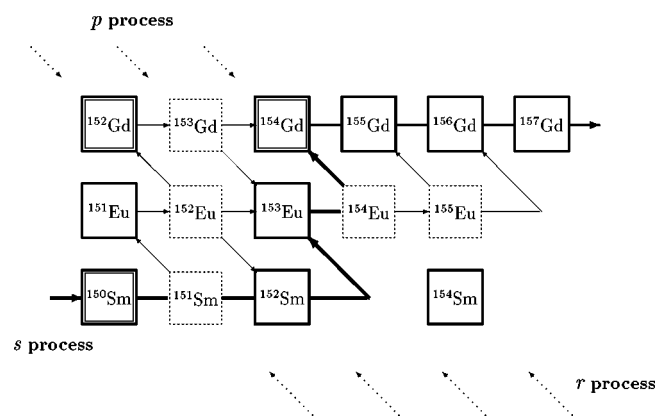(iv) Significant isotopic anomalies have been discovered

FIG. 1. The s-process reaction path in the Sm/Eu/Gd region with the important branchings at $A=151$ and 154.

in SiC grains from certain meteorites for several of the REEs [3–5]. If these anomalies can be confirmed to be of pure *s*-process origin, they can be used for probing the transport processed material to the stellar atmosphere and the resulting enrichment of the circumstellar envelope. For the identification of the *s* origin, accurate cross section data and the due consideration of possible branchings are mandatory.

In the course of a comprehensive *s*-process investigation of the REE region, so far 29 stellar (n, γ) cross sections have been determined with significantly improved accuracy using the Karlsruhe $4\pi \text{BaF}_2$ detector [6–10]. In addition, five stable [11,12] and two radioactive [13,14] isotopes were investigated by activation in a quasistellar neutron spectrum. This data set was complemented by statistical model calculations based on a consistent local parameter systematics [15].

In the present work, cross section measurements on $^{152,154}\text{Sm}$, $^{151,153}\text{Eu}$, and $^{164,170}\text{Er}$ are reported which aim at resolving the differences and inconsistencies of previous data. In addition to these experiments, which are described in Secs. II and III, improved Hauser-Feshbach calculations were performed with updated input parameters (Sec. IV). The impact of these results on the *s*-process branchings at ^{151}Sm and ^{154}Eu are discussed in Sec. V.

II. MEASUREMENTS

The measurements were carried out with the activation technique by irradiating sets of Sm, Eu, and Er samples in a quasistellar spectrum as described elsewhere [11,16]. The neutron spectrum was obtained by bombarding 30 μm thick metallic lithium targets with protons of 1912 keV energy, 31 keV above the reaction threshold of the $^7\text{Li}(p,n)^7\text{Be}$ reaction, which then yields a continuous neutron energy distribution with a high energy cutoff at $E_n = 106$ keV. The resulting neutrons are emitted into a forward cone with 120° opening angle. The angle-integrated spectrum peaks at 25 keV and exhibits almost exactly the shape required to determine the proper cross section average $\langle \sigma v \rangle / v_T$ corresponding to the stellar cross section for a thermal energy of $kT = 25 \pm 0.5$ keV [17]. Hence, the reaction rate measured in that spectrum yields immediately the stellar cross section at the respective temperature. Detailed information on the present work can be found in Refs. [18,19].

A. Samples

All Sm, Eu, and Er samples were prepared from oxide powder. In order to eliminate adsorbed water and to stabilize this fairly hygroscopic material, the powder was heated to 1300 K for 1 h, then pressed to thin pellets, which were again heated to 1300 K for another hour. After this treatment, the sample weight was repeatedly determined with a microbalance and was found to be constant throughout the measurements, at least within the ± 10 μg uncertainty of the balance.

For the samarium samples isotopically enriched material was available containing 99.0 ± 0.2 and $98.6 \pm 0.2\%$ ^{152}Sm and ^{154}Sm, respectively. The europium oxide was specified

with a chemical purity of 99.99%. Since relatively large uncertainties of 3 and 1.5 % [20,21] are assigned for the isotopic composition of natural Eu, the sample material was characterized by mass spectroscopy to contain 47.9 $\pm 0.3\%$ ^{151}Eu and $52.1 \pm 0.3\%$ ^{153}Eu. For the Er activations, ten samples were prepared, seven for the determination of the ^{170}Er and three thinner samples for the ^{164}Er cross section. The respective uncertainty in the isotopic composition of 1.3% was adopted from Ref. [22].

For all studied isotopes, the sample dimensions were varied with respect to diameter and thickness (Table I). This principle of modifying the relevant parameters was considered as an important test for the respective corrections and for a quantitative estimate of the related systematic uncertainties. With the different sample dimensions, the geometric effect of the divergent neutron field and the absorption losses in the subsequent activity measurement could be checked in this way. In order to keep the absorption losses small, relatively thin samples had to be used for the two samarium isotopes and for ^{164}Er, since the induced activities were characterized by soft γ radiation and by x rays in the latter case (Table II).

B. Irradiations and activation measurements

The experimental setup was the same as reported previously (Ref. [11], and references therein). The activations were carried out at the Karlsruhe 3.7 MV Van de Graaff accelerator with beam currents between 70 and 140 μA. The investigated Sm, Eu, and Er samples were sandwiched between 0.03 mm thick gold foils of the same diameter for normalization to the well-known (n, γ) cross section of ^{197}Au (648 ± 10 mb at $kT = 25$ keV). This normalization accounts directly for the definition of the stellar cross section; to obtain the straight spectrum-averaged cross sections, the present results have to be multiplied by a factor $\sqrt{\pi}/2$ (for details see [17]).

In all activations the neutron yield was continuously monitored in intervals of 20 s by a ^6Li glass detector at ~ 1 m distance from the target. This information allowed to correct the fraction of activated nuclei, that decayed already during the irradiation, for a possible time-dependence of the neutron yield. This correction can be significant if the irradiation time is comparable to or longer than the half-life of the induced activity and if this half-life differs from the gold standard. Accordingly, different irradiation times were chosen to control this correction (Table I).

The induced γ activities were counted by means of a shielded 76 cm^3 high purity Ge-detector (HPGe) with 1.7 keV resolution at 1.33 MeV γ-ray energy. The counting geometry was defined by a special adapter to the detector cap, by which the samples were positioned at a distance of 80 mm from the detector. The detection efficiency, which peaked near 60 keV, was determined in the relevant energy range between 15 and 1408 keV to $\pm 1.5\%$ by a set of calibrated sources.

The induced activities of the isotopically enriched samarium samples are characterized by relatively soft γ spectra. As an example, Fig. 2 shows the spectrum measured

TABLE I. Activations and sample characteristics.

Isotope	Activation	Irradiation Time (h)	Diameter (mm)	Samples Thickness (mm)	Total mass (mg)
^{152}Sm	SM1	15.9	6	0.2	28.6±0.01
	SM2	9.5	6	0.4	47.9±0.01
	SM3	6.1	6	0.4	47.0±0.01
^{154}Sm	SM4/SM4a	0.3 / 0.7	6	0.4	49.8±0.01
	SM5/SM5a	0.3 / 0.7	6	0.8	98.5±0.01
	SM6/SM6a	0.3 / 0.7	6	0.7	83.8±0.01
^{151,153}Eu	EU1	16.8	10	1.0	328.1±0.01
	EU2	10.0	5	1.1	93.6±0.01
	EU3	16.7	10	1.0	313.7±0.01
	EU4	7.8	5	1.2	100.9±0.01
^{164}Er	ER1	5.2	6	0.2	30.0±0.01
	ER2	5.3	6	0.2	30.1±0.01
	ER3	3.4	6	0.2	30.3±0.01
^{170}Er	ER4	7.2	6	0.7	91.4±0.01
	ER5	14.0	6	0.4	52.7±0.01
	ER6	4.9	6	0.4	53.6±0.01
	ER7	12.2	6	0.5	61.3±0.01
	ER8	6.4	10	0.6	221.4±0.01
	ER9	4.8	10	0.5	169.8±0.01
	ER10	4.6	10	0.6	208.2±0.01

after activation SM2. Only the transitions marked by arrows could be used for analysis since the intensities of the weak lines between the peaks at 69.7 and 97.4 keV are rather uncertain. The remaining line at 122 keV is due to an isotopic impurity.

Immediately after the europium activations, the induced activities exceeded 10^6 Bq and were dominated by the decay of the first isomer in ^{152}Eu. Of the six prominent lines in this decay, the well known transitions with 344, 842, and 963 keV energy were used to determine the partial (n,γ) cross section for populating this isomer. Subsequent to the measurement of the partial cross section a waiting time of 10 days corresponding to 25 half-lives of the isomer was observed before counting the low activities from the decay of the long-lived ground states. One of these spectra, which were accumulated over 40 to 70 h, is shown in Fig. 3. Downward and upward arrows indicate the respective ^{152}Eu and ^{154}Eu lines which were used in data analysis. All remaining lines were not considered since they are either too weak or too uncertain.

The analysis of the erbium activations ER1 to ER7 for obtaining the ^{170}Er cross section was based on the strongest γ-ray line at 308.3 keV since the other transitions are much weaker and more uncertain. In case of ^{164}Er, there are no γ transitions in the EC decay of ^{165}Er. Accordingly, the induced activities had to be determined via the emitted Ho-x

rays as shown in Fig. 4. Since natural erbium samples were used in the activations, the decay of the coproduced heavier Er isotopes gives rise to corresponding x-ray lines from the decay of their respective Tm daughters. The separation of the Ho-$K\alpha$ line from this Tm feature reveals an additional component from the x-ray fluorescence effect in the Er sample itself. The correction of the Ho line for the contribution from neutron captures in ^{162}Er could be minimized because of its shorter half life of 1.25 h. After waiting times of about 10 h between activation and counting the corresponding corrections were smaller than 0.5%. Since the resolution was not sufficient to resolve the $K_{\alpha 1}$ and $K_{\alpha 2}$ lines, the sum of their intensities was used in the analysis. In total, nine, four, and ten activations were carried out with the Sm, Eu, and Er samples, respectively (Table I).

III. EXPERIMENTAL CROSS SECTIONS

A. Data analysis

The net counts C_γ of a particular γ-ray line in the spectra taken with the HPGe detector can be expressed as

$$C_\gamma = A K_\gamma \epsilon_\gamma I_\gamma f_w f_m, \qquad (1)$$

where A denotes the total number of activated nuclei at the end of irradiation. The corrections for γ-ray self-absorption

TABLE II. Decay properties of the product nuclei.

Product nucleus	Half-life	γ-ray energy [a] (keV)	Intensity per decay (%)
^{153}Sm	1.946 ± 0.004 d	69.7	5.25 ± 0.25 [b]
		97.4	0.73 ± 0.02 [b]
		103.2	28.30 ± 0.60 [b]
^{155}Sm	22.3 ± 0.2 min	104.3	74.6 ± 1.9 [c]
		141.4	1.97 ± 0.08 [c]
^{152m1}Eu	9.274 ± 0.009 h	344.3	2.44 ± 0.30 [d]
		841.6	14.6 ± 2.1 [d]
		963.4	12.0 ± 1.7 [d]
^{152gs}Eu	13.542 ± 0.010 yr	244.7	7.49 ± 0.13 [d]
		344.3	26.6 ± 0.28 [d]
		778.9	13.79 ± 0.13 [d]
		964.1	14.34 ± 0.20 [d]
		1112.1	13.5 ± 0.2 [d]
		1408.0	20.87 ± 0.11 [d]
^{154}Eu	8.593 ± 0.004 yr	247.9	6.91 ± 0.05 [e]
		591.8	4.96 ± 0.04 [e]
		723.4	20.11 ± 0.14 [e]
		756.8	4.54 ± 0.04 [e]
		873.2	12.20 ± 0.08 [e]
		996.3	10.53 ± 0.07 [e]
		1004.8	17.90 ± 0.11 [e]
		1274.5	34.5 ± 0.26 [e]
^{165}Er	10.36 ± 0.03 h	$K_{\alpha 1}$ 47.55	38.32 ± 0.4 [f]
		$K_{\alpha 2}$ 46.70	21.50 ± 0.4 [f]
^{171}Er	7.52 ± 0.03 h	308.3	64.4 ± 2.5 [g]
^{198}Au	2.696 ± 0.002 d	411.8	95.5 ± 0.1 [h]

[a]Prominent γ-ray lines used in data analysis.
[b]Reference [71].
[c]Reference [49].
[d]Reference [45].
[e]Reference [48].
[f]Reference [36].
[g]Reference [72].
[h]Reference [73].

K_γ were calculated with the absorption coefficients of Ref. [23], and were always smaller than 2.5%. The only exceptions were soft γ lines at 141 keV from ^{155}Sm and at 69.7 keV line from ^{153}Sm which required corrections between 4.3 and maximal 20 %, respectively. A similar correction of 22% had to be applied in case of the 47 keV x-ray lines from ^{165}Er. The efficiency of the HPGe detector ϵ_γ was measured

to $\pm 1.5\%$, and the relative γ-ray intensities per decay I_γ were adopted from literature (Table II). The time factors $f_w = e^{-\lambda t_w}$ and $f_m = (1 - e^{-\lambda t_m})$ account for the fraction of nuclei that decay during the waiting time between activation and counting and during the measurement itself [16], and λ is the decay constant of the respective product nucleus. Cor-
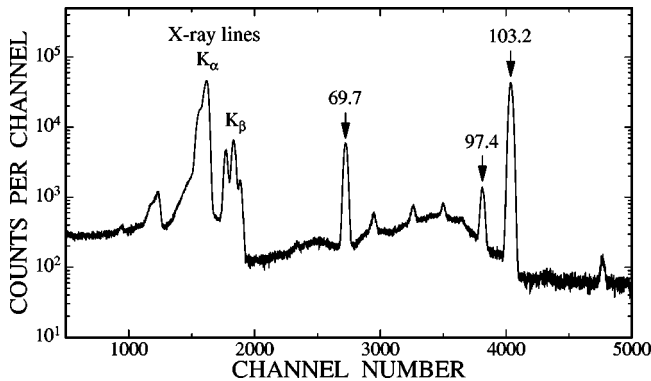

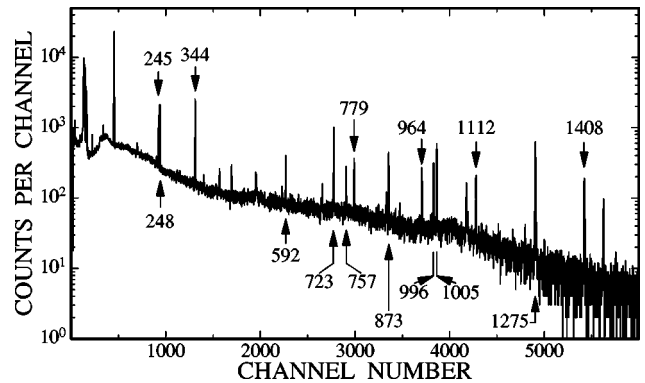FIG. 2. The γ-ray spectrum of the activated ^{152}Sm sample after activation SM2.

FIG. 3. The γ-ray spectrum of the activated europium sample after activation EU1. Lines from the decay of ^{152}Eu and ^{154}Eu are indicated by downward and upward arrows, respectively.
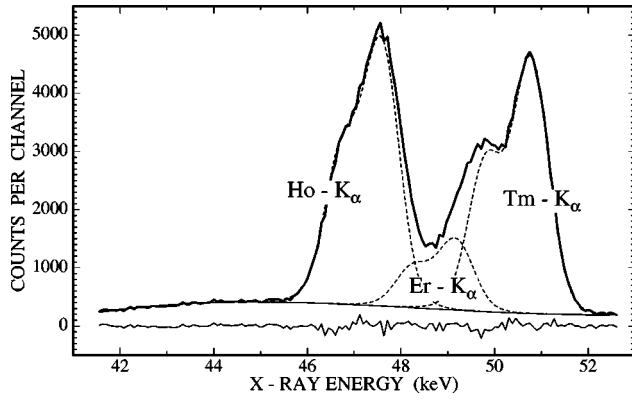
FIG. 4. The x-ray spectrum of the activated erbium sample after activation ER1. The Ho-K_α doublet from the decay of ^{163,165}Er can be well separated from the corresponding Tm component due to the ^{169,171}Er decays and also from the Er fluorescence lines. The quality of the fit is indicated by the difference spectrum.

rections for coincidence summing were always less than about 1% due to the small γ-ray efficiency and are, therefore, not listed explicitly. The total number of activated nuclei A is given by

$$A = \Phi_{\text{tot}} N \sigma f_b, \qquad (2)$$

where $\Phi_{\text{tot}} = \int \Phi(t) dt$ is the time-integrated neutron flux, N the sample thickness, and σ the spectrum-averaged neutron capture cross section. The time factor f_b corrects for the decay during activation, including the effects due to time variations of the neutron flux (for a definition see Ref. [16]). Since the integrated neutron flux is determined by the gold foils on both sides of the investigated sample, corrections for

target geometry as well as for neutron scattering and self-shielding are accounted for by averaging the induced activities of the two gold foils. Hence, the ratio for induced activities in the respective target and reference samples is given to very good accuracy by

$$\frac{A_i}{A_{\text{Au}}} = \frac{\sigma_i N_i f_{b,i}}{\sigma_{\text{Au}} N_{\text{Au}} f_{b,\text{Au}}} . \qquad (3)$$

In case of ^{152}Eu activity, the different components from the partial cross sections to the isomer and the ground state could easily be distinguished by the very different half-lives of 9.3 h and 13.5 yr.

B. Discussion of uncertainties

The experimental uncertainties are summarized in Table III where the investigated reactions are indicated by the respective product nuclei. For ^{151}Eu the partial cross sections to the isomer and to the ground state in ^{152}Eu are listed separately.

Significant contributions to the overall uncertainty originate from the gold reference cross section, the efficiency of the HPGe detector, and from the difference in neutron flux as measured by the two gold foils. The samarium cross sections and—in particular—the partial cross section to the isomer ^{152m}Eu are strongly affected by large uncertainties of the respective γ intensities (Table II). Any improvement of these data would, therefore, be important. The effect of the divergent neutron flux was estimated from the activities of the gold foils, 20% of that difference being assumed as the corresponding uncertainty.

TABLE III. Compilation of uncertainties.

Source of uncertainty	^{198}Au	^{153}Sm	^{155}Sm	^{152m1}Eu	$^{152\text{g.s.}}$Eu	^{154}Eu	^{165}Er	^{171}Er
				Uncertainty (%)				
Gold cross section	1.5							
Isotopic composition	0.1	0.2	0.2	0.3	0.3	0.3	1.3	1.3
Time factors f_w, f_m, f_b								
Counting statistics	0.3	0.1	0.1	0.4	0.4	0.3	0.4	0.2
Self-absorption K_γ		0.8	0.8	0.3	0.3	0.3	2.5	0.2
Efficiency ratio relative to Au γ rays		1.5	1.5	1.5	1.5	1.5	1.5	1.5
Gamma-ray intensity per decay I_γ	0.1	2.1	2.6	12.4	0.5	0.7	0.4	2.5
Difference in neutron flux		<1.5	<1.5	<1.5	<1.5	<1.5	<1.5	<1.5
Spectrum cutoff at 106 keV			1.0	0.5	0.5	0.5	0.5	0.5
Total uncertainty($kT=25$ keV)								
SM1-3		3.6						
SM4-6 and 4a-6a			4.0					
EU1-4				12.7	2.8	2.8		
ER1-3							3.9	
ER4-10				12.7	2.8	2.8		3.9
Extrapolation to $kT=20$ and 30 keV	0.5	2.0	0.5	2.0	0.5	0.5		
Extrapolation to $kT=10$ and 50 keV	1.0	4.0	1.0	4.0	1.0	1.0		

Though the experimental spectrum represents a very good approximation of the thermal situation, the cutoff at 106 keV requires a small correction if the investigated cross sections exhibit a different energy dependence than the gold reference cross section. This problem of the cross section shape affects also the extrapolation of the measured 25 keV cross sections to other thermal energies, in particular to $kT = 30$ keV, which is commonly used for the comparison of *s*-process data. Since differential (n, γ) cross sections $\sigma_{n,\gamma}(E_n)$ were available for ^{152}Sm [6], for both europium isotopes [24], and for ^{170}Er [25], the correction for the spectrum cutoff could be determined reliably in these cases. For ^{154}Sm and ^{164}Er, differential data were still missing. Therefore, the theoretically predicted energy dependence [26] was adopted in both cases, resulting in a correspondingly larger uncertainty for this correction. Since the statistical uncertainties from the activity measurements were practically negligible, the final uncertainties are determined by systematic effects and are, therefore, comparable to those of the individual activations.

C. Results and comparison with previous data

The cross sections obtained in the various activations are summarized in Table IV. In all cases, the differences among these results are well within the estimated uncertainties, thus confirming the procedures applied in data analysis. The cross sections from this work are compared with previous data in Figs. 5–10 where experimental and calculated values are indicated by black and open squares, respectively.

In case of ^{152}Sm (Fig. 5) the present value is somewhat lower than the accurate measurement of Ref. [6] but still compatible within a 2σ error band. The cross section given in Ref. [25] is certainly too large and can be ruled out, whereas the first measurement [27] agrees quite well. For ^{154}Sm (Fig. 6) there are few experimental results. While the oldest measurements suffer from large uncertainties, the value of Ref. [25] appears again too large, indicating a systematic effect in this experiment, possibly due to a contamination of the sample by adsorbed humidity [28] or by a small Eu impurity.

The numerous, previous measurements of the large europium cross sections exhibit significant discrepancies (Figs. 7,8). For both stable isotopes, the present results confirm the most recent data [24,29,30], whereas all data obtained in the seventies [31–33] are systematically too high, possibly also due to unnoticed humidity in the samples. The relatively large uncertainty of the present activation is caused by the very uncertain γ-ray intensity in the decay of the first isomer ^{152m1}Eu.

In case of ^{164}Er the cross section (Fig. 9) was found much larger than reported in the only previous measurement [34]. Most of this difference of about 35%—which bears important consequences for the extrapolation to the unstable, protorich nuclei of relevance for the *p* process [35]—could be explained by the fact that the presently adopted x-ray intensities [36] are 25% lower. In view of the remaining discrepancy, a series of four activations was carried out to verify the treatment of corrections and the evaluation of systematic uncertainties. In this context, it is important to note that activa-

tions with the same samples resulted in ^{170}Er cross sections which are perfectly consistent and in good agreement with previous data [25,37] (see Fig. 10). Another improvement compared to Ref. [34] was that the spectra were analyzed with a special code which allowed to fit the x-ray line shapes properly [14].

Figures 5–10 include the previous cross section calculations of Refs. [38,39] with estimated uncertainties of typically 50%. In general, these values are in fair agreement with the present measurements, except for the samarium cross sections of Harris [39], which are two times larger than the experimental data.

IV. STATISTICAL MODEL CALCULATIONS

Refined statistical model calculations have been performed on the basis of a *local* systematics of the relevant model parameters in the mass range of interest, including as much experimental information as possible. This set of parameters is required to be internally consistent, and the spread of the data in this systematics compared to a smooth trend with mass number can be used to obtain realistic estimates for the related uncertainties. The respective parameters for the isotopes of interest can then be *interpolated* with some confidence. This concept and the related techniques have been described extensively in previous publications [40,41]. In the following, the discussion is restricted to the particular problems of the present cases, and to the adopted parametrization.

A. Evaluation of model parameters

The previous parameter systematics of the Sm-Eu-Gd region [42] was updated for the europium isotopes by an analysis of the available experimental information. In particular, neutron resonance schemes and discrete level information were considered in detail in order for achieving a realistic level density description. Neutron resonance schemes were also used for deriving the s-wave strength functions for characterizing the entrance channel as well as the competition among the exit channels.

Neutron resonances. Due to the limited ensemble of observed resonances [43], several statistical methods (missing level estimator, truncated and segmented Porter-Thomas distributions, stair case plots) were used to determine the average level spacings $\langle D_{obs} \rangle$, the average neutron widths $\langle \Gamma_n \rangle$, and the *s*-wave strength functions S_0. The analysis was carried out in an iterative way until the different methods converged to a consistent parameter set. This technique could only be applied to statistically significant samples such as ^{151}Eu and ^{153}Eu, otherwise reliable results could not be obtained.

Level densities. The combination of the average level spacings $\langle D_{obs} \rangle$, with the information from discrete level schemes represents the necessary input for the Gilbert-Cameron approach of the level density. The level schemes for the europium isotopes are well investigated and fairly comprehensive [44–49]. In principle, this should provide a sufficient basis for deriving reliable level densities. However, if this information is used to calculate the total radiative

TABLE IV. Measured stellar (n,γ) cross sections compared with previous data.

Thermal Energy (keV)	$\dfrac{\langle\sigma v\rangle}{v_T}$ (mb)						
	^{152}Sm	^{154}Sm	^{151}Eu$\rightarrow^{152m1}$Eu	^{151}Eu$\rightarrow^{152\text{g.s.}}$Eu	^{153}Eu	^{164}Er	^{170}Er
			Previous data				
30	378±23 [a]	293±19 [a]	1545±173 [a]	4367±175 [a,b]	3170±317 [a]	714±61 [a]	223±33 [a]
	445±25 [d]				2630±200 [c]		
	473±4 [e]				2447±73 [d]		
			This work				
25							
SM1	473±17						
SM2	467±17						
SM3	480±17						
SM4		218±9					
SM4a		235±10					
SM5		237±10					
SM5a		225±9					
SM6		218±9					
SM6a		224±9					
EU1			1539±195	2423±75	2771±86		
EU2			1586±201	2521±78	2965±92		
EU3			1584±201	2558±79	2905±90		
EU4			1597±203	2579±80	3024±94		
ER1						1093±49	179±8
ER2						1113±42	186±8
ER3						1048±48	174±8
ER4							182±11
ER5							173±8
ER6							173±8
ER7							175±9
ER8							176±8
ER9						976±74	179±8
ER10							177±8
Mean value	473±17	226±9	1577±200	2520±71	2917±82	1075±45	177.7±7
30 [f]	431±16	206±9	$\sigma_{\text{tot}}(^{151}\text{Eu}) = 3736\pm210$		2710±77	1084±51	170±7

[a]Reference [53] (recommended values based on all references before 1987).
[b]Sum of partial cross sections to ground state and isomer.
[c]Reference [29].
[d]Reference [30].
[e]Reference [6].
[f]Extrapolated from the measured 25 keV values (see text and Table III).

width according to the prescription of Ref. [50], it turned out that the experimental data [43] could only be reproduced for ^{154}Eu and ^{156}Eu. For the other investigated isotopes, these results were 20 to 50 % smaller than the experimental data. This discrepancy is confirmed by the behavior of the level density parameter a, the matching energy U_x, and the nuclear temperature T_{nucl}, which were derived in this analysis as well. Also these values exhibit an irregular spread compared to the well established overall systematics of Ref. [42]. Therefore, an alternative approach was used as described in the following section.

B. Calculated cross sections

In view of these rather unexpected problems, the optical model Hauser-Feshbach (HF) prescription by the code CERBERO[1] [51] could be adopted only for the odd-odd europium nuclei. For ^{151}Eu, ^{153}Eu, and ^{155}Eu, these results were complemented by a set of additional calculations with a strength function model including width fluctuation correc-
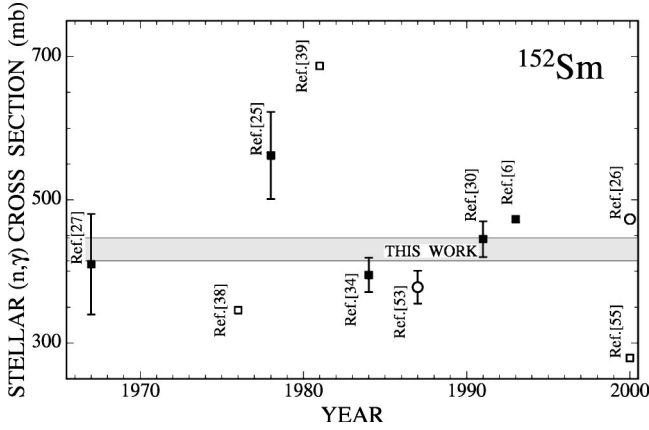
_____

[1]Available from the OECD NEA Data Bank, Paris.

FIG. 5. The 30 keV (n,γ) cross section of ^{152}Sm (extrapolated from the measured 25 keV data, shaded band) compared to previous measurements (black squares), theoretical calculations (open squares), and evaluated data (open circles).

FIG. 7. The 30 keV (n,γ) cross section of ^{151}Eu (extrapolated from the measured 25 keV data, shaded band) compared to previous measurements (black squares), theoretical calculations (open squares), and evaluated data (open circles).

tions (code SAUD [52]). In this approach the persisting uncertainties of the statistical model parameters (Table V) can be avoided by using experimentally determined quantities, such as the strength functions S_0, S_1, radiative widths Γ_γ, and observed level spacings $\langle D_{\mathrm{obs}} \rangle$ (Table VI). In the present case, the strength functions were derived from the systematic trends of different evaluations [15,43].

The comparison of these calculations with the differential cross sections reported in Ref. [24] showed that only the strength function model yields a satisfactory description of the cross section shape up to 1 MeV neutron energy, whereas the HF results tend to overestimate the competition by neutron inelastic channels above E_{cut}, where the level density treatment changes from the known discrete levels to a level continuum. For most of the investigated europium isotopes this critical transition occurs between 300 and 400 keV. Therefore, the present calculations were considered only up to 400 keV, being aware that the proper treatment of the inelastic channel at higher energies requires detailed coupled channel calculations. With this restriction the results ob-
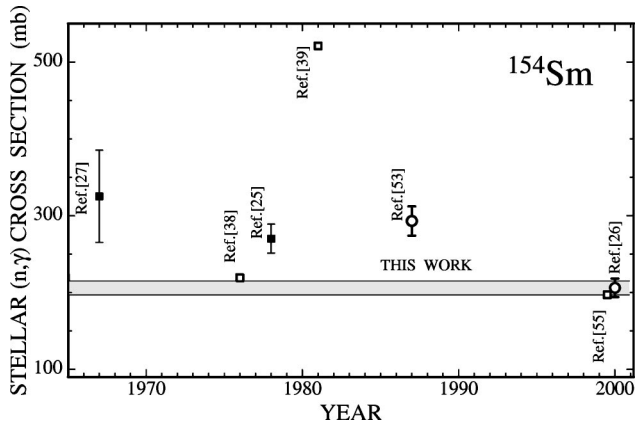
tained with the HF approach were preferred over the more schematic strength function model. For these results a 20% uncertainty was estimated at typical *s*-process energies.

The calculated ground state cross sections at kT $=30$ keV are summarized in Table VII. Comparison with the experimental data of Table IV shows that the present Hauser-Feshbach results obtained with local parameters as well as the NON-SMOKER values based on a global parameter set [48] describe the general trend with neutron number correctly whereas previous calculations [38,39,53] are systematically underestimating the ^{151}Eu cross section and are too high for ^{155}Eu. The only problem with the NON-SMOKER calculation refers to ^{151}Eu, which is underestimated due to a local deficiency of the finite range droplet model (FRDM) [54]. The FRDM, which is used as input to define the microscopic correction in the global level density description, shows fluctuations in the reliability of predicting shell and pairing corrections. In a previous cross section compilation [53] the NON-SMOKER cross sections had been corrected for

FIG. 6. The 30 keV (n,γ) cross section of ^{154}Sm (extrapolated from the measured 25 keV data, shaded band) compared to previous measurements (black squares), theoretical calculations (open squares), and evaluated data (open circles).
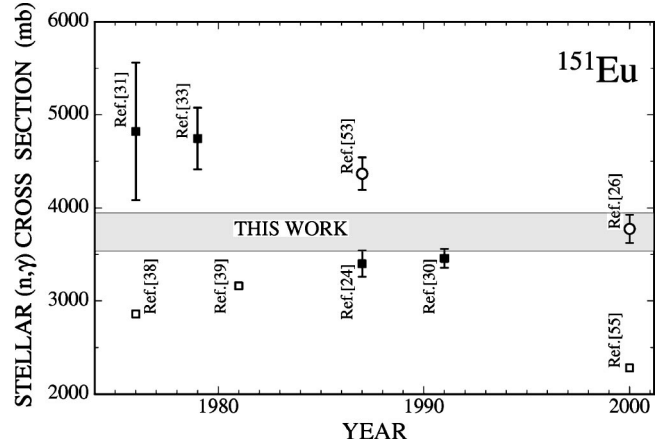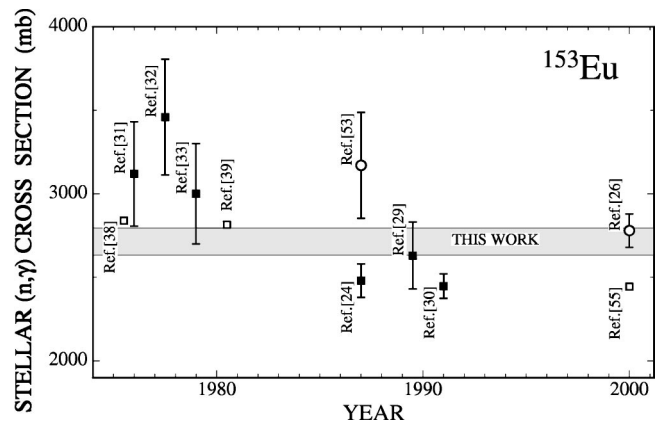

FIG. 8. The 30 keV (n,γ) cross section of ^{153}Eu (extrapolated from the measured 25 keV data, shaded band) compared to previous measurements (black squares), theoretical calculations (open squares), and evaluated data (open circles).
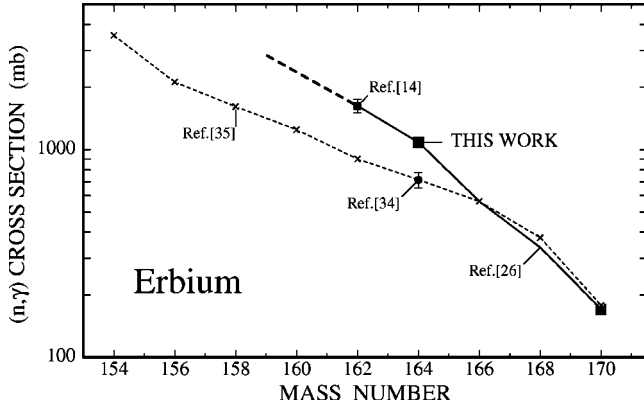
FIG. 9. The 30 keV (n,γ) cross section of ^{164}Er (extrapolated from the measured 25 keV data) compared to those of the stable even Er isotopes illustrating the smooth trend with mass number. This complete set of experimental data represents an important test of theoretical cross section predictions for neutron deficient nuclei in the *p*-process region (indicated by the dashed line). Previous calculations of Rayet [35], which were guided by the superseded ^{164}Er cross section, led to an unrealistic extrapolation (crosses).

these input deficiencies as a function of neutron number. These corrections to the NON-SMOKER cross sections yields a ^{151}Eu cross section of 3920 mb, in excellent agreement with the experimental result, but are small for the heavier Eu isotopes.

C. Stellar enhancement factors

Many isotopes in the investigated mass region exhibit excited states at sufficiently low energies which are significantly populated at *s*-process temperatures. This means that their (n,γ) cross sections contribute to the Maxwellian average and have to be considered accordingly. This effect is described by the ratio of the effective stellar average and the corresponding ground state value. Such stellar enhancement factors $\text{SEF}=\langle\sigma\rangle^{\text{star}}/\langle\sigma\rangle^{\text{lab}}$ are expected to be much less un certain than the cross sections themselves since part of the theoretical uncertainties cancel out in the ratio.
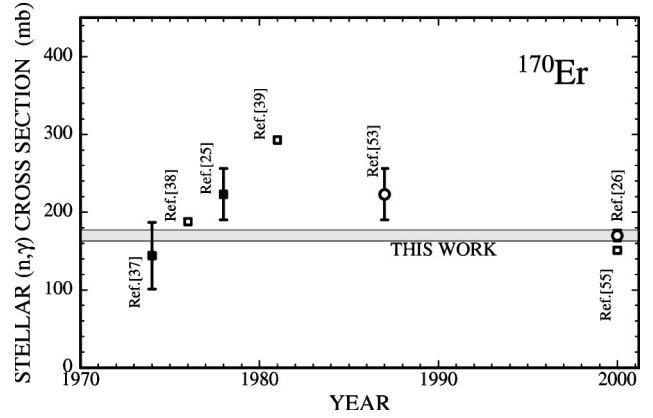

FIG. 10. The 30 keV (n,γ) cross section of ^{170}Er (extrapolated from the measured 25 keV data, shaded band) compared to previous measurements (black squares), theoretical calculations (open squares), and evaluated data (open circles).

In view of discrepant predictions in previous calculations [38,39], the present study includes also the (n,γ) cross sections of the first five excited states in each target nucleus. In these cases, the superelastic channel that accounts for neutron scattering to one of the lower states (where the scattered neutrons gain in energy) was properly taken into account. The effective Maxwellian average cross sections were obtained by weighting the values for the excited states with the respective population probabilities.

The resulting enhancement factors for a thermal energy of $kT=30$ keV are compared in Fig. 11 and in Table VIII with the corresponding values obtained with the NON-SMOKER code using a global parametrization [55]. Figure 11 includes also the results of previous calculations [38,39]. The present calculation yields a reduction rather than an enhancement of the cross sections under stellar conditions. This appears plausible since the comparably large ground state spins of the investigated europium isotopes imply that the excited state cross sections are determined by average statistical weights only. Therefore, the competition by superelastic scattering accounts for the smaller effective cross sections under stellar

TABLE V. Level density parameters for the HF calculations with the code CERBERO.

| | Compound nucleus | | | | | |
	^{151}Eu	^{152}Eu	^{153}Eu	^{154}Eu	^{155}Eu	^{156}Eu
E_{cut} [a] (MeV)	0.360	0.285	0.400	0.110	0.330	0.050
a (MeV)$^{-1}$	23.0±5.0	24.8±0.5	23.0±0.3	23.2±0.3	21.2±0.6	22.5±0.4
U_x (MeV)	5.9±0.5	5.2±0.5	5.9±0.3	5.2±0.3	5.5±0.6	4.4±0.5
T_{nucl} (MeV)	0.58	0.53	0.58	0.55	0.59	0.53
Deformation [b]	0.198	0.205	0.225	0.239	0.245	0.252
Spin cutoff factor [c]	7.8	9.6	13.3	9.7	13.3	7.4
$\langle D_{\text{obs}}\rangle$ (eV)	3.2 [d]	0.7±0.1	0.25±0.04	1.2±0.3	0.9±0.1	2.1 [d]
Γ_γ (meV)		97±10	160±15	110±15	140±20	100±15

[a]Below this energy the known discrete levels were considered explicitly.
[b]Reference [74].
[c]Derived via maximum likelihood analysis of the experimental spin distributions of discrete levels.
[d]Adopted from systematics [42].

TABLE VI. Evaluated strength functions for the SFM calculations with the code SAUD.

	Target nucleus				
	^{151}Eu	^{152}Eu	^{153}Eu	^{154}Eu	^{155}Eu
$S_0 \times 10^4$	4.0±0.5	3.6±1.2	2.4±0.3	1.8±0.2	1.6±0.4
$S_1 \times 10^4$	0.57	0.57	0.58	0.59	0.59

conditions. While the older calculations [38,39] do not exhibit significant variations with mass number, the new data (this work and the NON-SMOKER results [55]) show more pronounced trends with a different odd-even pattern.

With respect to the branching analyses these results have the following consequences. (i) The stellar enhancement factors of the stable isotopes exhibit differences of 10%. If this is adopted as the remaining uncertainty, it determines the uncertainty of the corresponding *s* abundances. But since the *s* components of the total abundances are small, this uncertainty does not affect the *r*-process distribution. (ii) The fair agreement for the branch point nuclei, on the other hand, shows that the 20% uncertainties estimated for the ground state cross sections can also be adopted for the stellar values.

D. Adopted cross sections and decay rates

The present results and the information from literature was used to obtain a best set of stellar cross sections in the investigated mass region $150 \leq A \leq 156$. For the stable Sm, Gd, and Dy nuclei, the recommended stellar cross sections of a recent tabulation [26] have been adopted. This holds true for the ^{151}Eu and ^{153}Eu cross sections as well, which had been included in this tabulation.

For the unstable isotopes a single experimental value was available for ^{155}Eu [13]. In this case, additional systematic uncertainties of 2.5, 5, 7.5, and 10 %, have been assumed for the extrapolation to thermal energies of 25, 20, 15, and 10 keV, respectively. The missing cross sections of the branch point nuclei ^{152}Eu and ^{154}Eu were derived from calculated data. In Fig. 12 the adopted values of the stable europium isotopes are compared with the present calculations and other results [38,39,55]. Since the present calculation yields a better description of the cross section trend with neutron number, these values were adopted for ^{152}Eu and ^{154}Eu. For the two minor branch points ^{153}Sm and ^{153}Gd, the recommended cross sections of Ref. [26] were used, which reproduce the experimentally known cross sections of the neighboring isotopes within ±16 %.

TABLE VII. Calculated capture cross sections (mb).

Neutron energy (keV)	Ground state cross sections					
	^{151}Eu	^{152}Eu	^{153}Eu	^{154}Eu	^{155}Eu	Reference
1	38500	50000	33000	38300	15800	This work
10	8100	12700	6500	8250	2520	
20	4980	8300	3950	5100	1510	
25	4020	7200	3400	4380	1310	
30	3480	6400	3000	3870	1160	
50	2420	4650	2150	2800	860	
100	1630	2850	1320	1710	550	
200	1210	1550	710	700	280	
500	490	550	410	205	110	
700	360	350	305	140	85	
1000	260	230	220	90	60	
2000	135	95	110	35	32	
Thermal energy [a] ($kT=30$ keV)						
	3470	5981	2894	3703	1154	This work (local)
	2281	6309	2444	4169	1320	This work (global)
		7600		4420		[b]
	2860	5180	2840	4450	1730	[c]
	3161	4032	2814	2989	2088	[d]

[a]Thermal average of ground state cross sections.
[b]Reference [26].
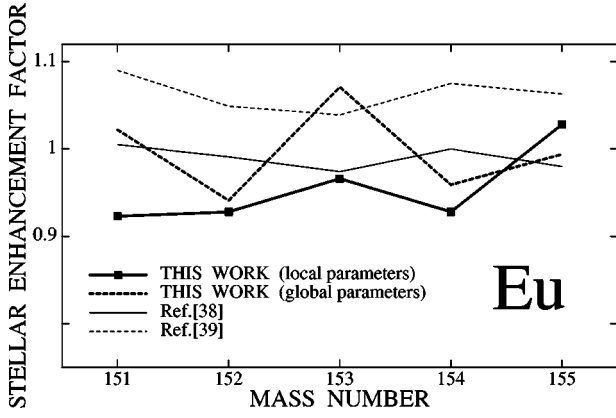[c]Reference [38].
[d]Reference [39].

FIG. 11. Stellar enhancement factors for (n,γ) cross sections of the europium isotopes for $kT = 30$ keV.

The cross section of the important branch point isotope ^{151}Sm was taken from a previous calculation [11] where the same technique of constructing a local parameter systematics was applied. This value, which is 40% smaller than the recommended cross section in Ref. [26], was combined with the stellar enhancement factor of Ref. [55]. The impact of this cross section uncertainty will be discussed below.

Another important note concerns the stellar enhancement factor of ^{164}Er. Existing calculations signify large differences, the results ranging from 1.06 [38], 1.12 [39], up to 1.24 [55], respectively. These differences bear significant consequences for the branching at $A = 163$ which testifies the electron density at the s-process site. The adopted stellar cross sections are summarized in Table IX.

The information on stellar β-decay rates for the proper description of the reaction flow at the branch points has been adopted from the tables of Ref. [56]. For both relevant branch point nuclei ^{151}Sm and ^{154}Eu, the enhancement of the decay rate is dominated by β decays from thermally populated excited states. In case of ^{151}Sm, about 85% of the enhancement are due to a single allowed transition from the fourth excited state at 92 keV to the first excited state in ^{151}Eu, whereas a number of transitions contribute to the stellar ^{154}Eu rate. Here, the first excited state at 68 keV provides
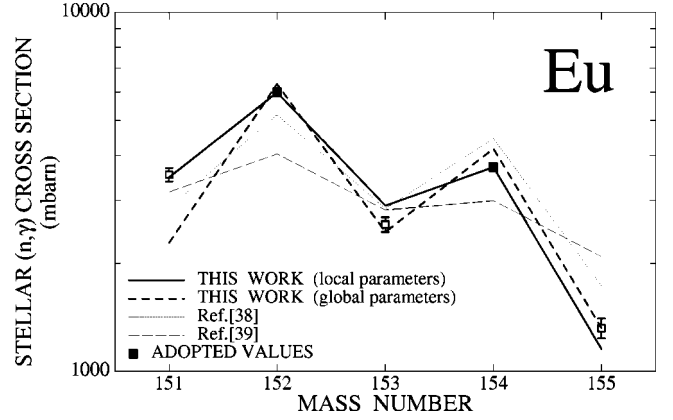

FIG. 12. The Maxwellian average cross sections of the europium isotopes for $kT = 30$ keV compared to calculated data sets. The open squares with error bars are experimental data corrected for stellar enhancement factors, the full squares are the adopted values for the unstable branch point nuclei.

the most important part. In addition, the ^{151}Sm rate is affected by bound state β decay which contributes a factor 2.5 to the enhancement, and by the electron density in the stellar plasma which causes a slight retardation of $\approx 20\%$. Both effects are negligible for ^{154}Eu due to the higher decay energy. At a typical s-process temperature of $3 \times 10^{8\circ}$, the decay is accelerated by factors of 30 and 300 for ^{151}Sm and ^{154}Eu, respectively.

V. ASTROPHYSICAL IMPLICATIONS

A. The s-process branchings at ^{151}Sm and ^{154}Eu

The s-process reaction flow in the Sm/Eu/Gd region exhibits a number of branching points as indicated in Fig. 1. The strength of these branchings is defined by the abundances of the s-only isotopes ^{152}Gd and ^{154}Gd, which are shielded against the β-decay chains from the r-process region by their samarium isobars.

TABLE VIII. Stellar enhancement factors.

| Target nucleus | Thermal energy (keV) | | | | | | Reference |
	10	15	20	25	30	40	
^{151}Eu	0.98	0.96	0.95	0.93	0.92		This work
	0.98	0.99	1.00	1.01	1.02	1.04	[a]
^{152}Eu	1.00	0.99	0.98	0.95	0.93		This work
	1.00	1.00	1.00	0.98	0.94	0.88	[a]
^{153}Eu	1.00	1.00	0.99	0.98	0.97		This work
	1.00	1.00	1.02	1.05	1.08	1.07	[a]
^{154}Eu	1.00	0.99	0.96	0.93	0.93		This work
	1.00	1.00	1.00	0.98	0.95	0.90	[a]
^{155}Eu	1.00	1.00	1.01	1.02	1.03		This work
	1.00	1.00	1.00	1.00	0.99	0.98	[a]

[a]Reference [55].

TABLE IX. Adopted Maxwellian averaged cross sections (mb).

| Isotope | Thermal energy (keV) | | | | | | Reference |
	10	15	20	25	30	40	
^{151}Sm	4065	2869	2198	1850	1585 ± 400	1286	[a, b]
^{151}Eu	7616	5645	4601	3896	3437 ± 200		This work [c]
^{152}Eu	11900	9207	7615	6403	5562 ± 1200		This work
^{153}Eu	4914	3906	3314	2920	2628 ± 80		This work [c]
^{154}Eu	7780	5910	4704	3906	3443 ± 750		This work
^{155}Eu	2830	2134	1764	1526	1360 ± 84		[d, b, c]

[a]Data of Ref. [11] complemented with SEF data from Ref. [55].
[b]Temperature dependence adopted from Ref. [26].
[c]Complemented with present SEF data.
[d]Data of Ref. [13] complemented with [b], [c].

Since the rare earth elements are chemically nearly identical, their abundance ratios are known to $\pm 1.3\%$ on average [57]. Hence, the following analyses can be normalized via the unbranched *s*-only isotope ^{150}Sm. This allows to treat the branchings to ^{152}Gd and ^{154}Gd independent of each other. Compared to a previous analysis [58], which concentrated on the ^{152}Gd/^{154}Gd ratio, this offers the advantage of separating the effects due to the stellar β-decay rates of the branch point nuclei from the *p*-process corrections and from a possible enhancement of the stellar neutron capture rate of ^{154}Gd [7].

The resulting *s* abundances of ^{152}Gd and ^{154}Gd are mainly determined by the branching points ^{151}Sm and ^{154}Eu. The branching at ^{155}Eu is required for determining the *s*-process abundance of ^{155}Gd, an important test for the identification of pure *s*-process gadolinium in meteoritic material. The additional branchings at ^{152}Eu and ^{153}Gd are too weak to produce a noticeable effect on the abundance pattern.

B. Abundances

The *s*-process calculations presented in the following were normalized to the solar abundance of ^{150}Sm. Though the solar abundances of Sm, Eu, and Gd are given with uncertainties of only 1.3, 1.6, and 1.4 % [57], an additional uncertainty arises from possible *p*-process contributions to the abundances of the *s*-only isotopes. An empirical estimate based on the abundances of nearby *p*-only isotopes suggests a large correction for ^{152}Gd of up to 50% [58]. However, improved calculations [59–61] have reported *p*-process yields of less than 12% for this isotope. The *p*-process yields for ^{154}Gd and ^{150}Sm are below 1.5 and 0.2 %, respectively [35], and, therefore, less critical. Another contribution to the ^{152}Gd abundance comes from the *s* process in massive stars, which is estimated to account for about 6% of the solar value [62].

Apart from the *p*-process corrections, there is also the problem of mass fractionation in the experimental determination of the isotopic composition [63]. This difficulty refers to the composition of solar gadolinium as well as to that of the meteoritic samples. Presently, the related corrections are still unknown, but a conservative assessment suggests an additional uncertainty of 0.6% for the isotopic ratio of ^{152}Gd and ^{154}Gd due to mass fractionation.

C. *s*-process models

Analyses of the *s*-process reaction flow in the Sm/Eu/Gd region were carried out by means of the classical approach and are compared with a stellar model for helium shell burning in low mass stars. Only a brief sketch of these models is given here since a more detailed description can be found elsewhere [64,65].

The purely phenomenological classical approach was formulated before stellar models for the helium burning stage were available [66,67]. Since then, it became a useful tool, not only for reproducing the *s* abundances but also for characterizing the physical conditions during the *s* process in an empirical way. Meanwhile, the two components of the classical approach could be assigned to stellar scenarios. The *weak* component, which is important in the mass range between Fe and Zr, was attributed to helium core burning in massive stars [62], while the *main* component occurs during helium shell burning in low mass stars and accounts for the *s* abundances in the mass range $A > 100$. For the main component, irradiation of an iron seed by an exponential distribution of neutron exposures was assumed. With the further assumption of a constant neutron density and temperature, the *s*-process reaction flow is characterized in this approach by the iterative expression

$$\langle \sigma \rangle N_s(A) = \frac{G N_\odot^{56}}{\tau_0} \prod_{i=56}^{A} \left(1 + \frac{1}{\sigma_i \tau_0} \right)^{-1}. \tag{4}$$

The two free parameters, the fraction G of the observed ^{56}Fe abundance required as seed, and the mean neutron exposure τ_0, are determined by fitting the empirical $\langle \sigma \rangle N_s$ values of those *s*-only isotopes that experience the entire reaction flow. For the present analysis,

$$\tau_0 = (0.296 \pm 0.003) \left(\frac{kT[\text{keV}]}{30} \right)^{1/2} \text{ mb}^{-1}, \tag{5}$$

has been adopted from Ref. [2], whereas G was defined by normalization to the $\langle \sigma \rangle N_s$ value of ^{150}Sm.

Branchings in the *s*-process path have to be treated separately [64,68] via the branching factors

$$f_\beta = \frac{\lambda_\beta}{\lambda_\beta + \lambda_n}, \tag{6}$$

$\lambda_\beta = \ln 2 / t_{1/2}$ and $\lambda_n = n_n \, v_T \, \langle \sigma \rangle$ being the rates for β decay and neutron capture. The relevant quantities in these expressions are the β half-lives $t_{1/2}$, the neutron density n_n, the mean thermal neutron velocity v_T, and the Maxwellian averaged capture cross section $\langle \sigma \rangle$. The adopted half-lives and Maxwellian averaged cross sections are discussed above, and the neutron density $n_n = (4.1 \pm 0.6) \, 10^8 \text{ cm}^{-3}$, was taken from Ref. [11].

The combined effect of the branchings in Fig. 1 can be deduced from the $\langle \sigma \rangle N_s$ ratios of the partially bypassed *s*-only isotopes ^{152}Gd and ^{154}Gd relative to ^{150}Sm, which is exposed to the entire *s*-process flow. Since the neutron density is defined by the branchings in the neodymium/promethium region, reproduction of the ^{152}Gd and ^{154}Gd abundances requires the proper choice of the effective stellar temperature via the temperature-dependent β-decay rates of the branch point isotopes, mainly of ^{151}Sm and ^{154}Eu.

Though the classical approach has been challenged by the recent improvement of stellar *s*-process models for low mass stars (see below) it is still a good approximation between magic neutron numbers. Current stellar models for describing the main *s*-process component in the mass range $A > 100$ refer to helium shell burning in thermally pulsing low mass AGB stars [69]. This scenario is characterized by the subsequent operation of two neutron sources during a series of subsequent helium shell flashes. First, the

^{13}C$(\alpha,n)^{16}$O reaction occurs under radiative conditions during the intervals between the He-shell burning episodes. While the ^{13}C reaction provides most of the neutron exposure at low temperatures ($kT\sim 8$ keV) and neutron densities ($n_n \lesssim 10^7$ cm^{-3}), the resulting abundances are modified by a second burst of neutrons from the ^{22}Ne$(\alpha,n)^{25}$Mg reaction, which is activated during the next convective instability, when high peak neutron densities of $n_n \lesssim 10^{10}$ cm^{-3} are reached at $kT\sim 23$ keV. Although this second burst accounts only for a few percent of the total exposure, it is essential for adjusting the abundance patterns of the s-process branchings.

Accordingly, the branchings can serve as sensitive tests for the interplay of the two neutron sources as well as for the time dependence of neutron density and temperature during the second neutron burst. In this context, it is important to note that the (n,γ) cross sections in Sm/Eu/Gd region are large enough that typical neutron capture times are significantly shorter than the duration of the two neutron exposures. Hence, the final abundance patterns are determined by the freeze-out conditions of the ^{22}Ne phase, regardless of the situation after the ^{13}C phase.

Such models were shown to exhibit remarkably similar conditions for a range of stellar masses ($1.5 \leq M/M_\odot \leq 3$) and metallicities ($-0.4 \leq$ [Fe/H] ≤ 0) [70]. The actual neutron-capture nucleosynthesis efficiency in each star depends on the metallicity, the choice of the amount of ^{13}C that is burnt, and its profile in the intershell region, i.e., what has become known as the ''^{13}C pocket.'' Since the formation of this pocket is difficult to describe in a self-consistent way, current calculations of AGB nucleosynthesis have still to be based on a plausible parametrization (see, e.g., Refs. [65,70]). The calculations cited below Ref. [2] refer to a model of 2 $M_\odot$ and a metallicity 0.5 $Z_\odot$, which can be considered as representative for the s-process conditions on the AGB, and has been shown to match the solar main s-process component fairly well.

D. Branching Analyses

Based on the improved cross section data a series of branching analyses has been carried to derive estimates for neutron density, temperature, and electron density by means of the classical model. These results are listed in Table X for two cross section sets. In the upper part, the present Eu data are combined with the Pm cross sections of Toukan *et al.* [11], all other values being adopted from the recent compilation of Bao *et al.* [26], whereas the lower part shows cases where all cross sections are taken from this compilation.

In runs 1 to 4 standard neutron density and temperature values of 4.1×10^8 cm^{-3} and $kT = 30$ keV were used. Variation of the electron density indicates that the critical ^{164}Er abundance can be best reproduced for $n_e = 6 \times 10^{26}$ cm^{-3} if a 6% fraction is allowed for the predicted p-process contribution. The response of the ^{152}Gd abundance to the electron density is considerably weaker. The comparably strong effect of temperature is illustrated in runs 3, 5, and 6 where small changes result in fairly large steps in the

^{152}Gd abundance. If an additional 20% contribution from the p process and from the s process in massive stars is considered, the ^{152}Gd abundance constrains the temperature to values near $kT = 30$ keV. Though variation of the neutron density in runs 4 and 7 to 9 has also a significant impact on the abundances of ^{152}Gd and ^{164}Er, these changes must be restricted to a narrow range of $(4.5 \pm 0.3) \times 10^8$ cm^{-3} because of the very well-defined ^{148}Sm abundance. These calculations show inherent problems since there is obviously no reasonable combination of parameters that can reproduce all four s-nuclei in the considered branchings. In particular, none of these cases produces enough ^{154}Gd and none can reconcile the ^{164}Er production (which favors higher neutron densities) without overproducing ^{148}Sm, which is defined with an uncertainty of 1%.

The lower part of Table X refers to calculations where the Pm cross sections of Toukan *et al.* [11] have been replaced by the significantly larger estimates suggested in Ref. [26]. The consequence of this change is obviously a corresponding reduction in neutron density, which must be compensated by lower temperatures and electron densities in order to accomodate the ^{164}Er abundance.

The sensitive influence of the ^{151}Sm cross section on the ^{152}Gd abundance is illustrated in the bottom line of Table X. The 50% increase in the ^{151}Sm cross section by replacing the adopted value [11] by that of Ref. [26] translates immediately into a corresponding 50% decrease in the ^{152}Gd abundance.

Obviously, none of the existing data sets does result in satisfactory solutions, a dilemma that underlines the importance of the cross sections for the unstable branch point nuclei ^{147}Pm, ^{148}Pm, and ^{151}Sm. Therefore, vigorous efforts are necessary towards direct measurements on these radioactive isotopes. Plans for such attempts exist presently for ^{147}Pm and ^{151}Sm. In addition to the mere cross sections, stellar enhancement factors represent another serious problem. The fact that recent predictions [26] differ significantly from earlier calculations [38], i.e., for the key isotope ^{164}Er, illustrates the need for more detailed theoretical studies as well as for complementing experiments.

An improved set of stellar (n,γ) data is not only needed to investigate the emerging inconsistencies of the steady classical s process in more detail [2], but are most important with respect to the yet uncertain stellar models for He burning in low mass AGB stars. The s-process branchings in the lanthanide region represent unique tests for these rather complex AGB models. For the example of the 2 $M_\odot$ mass model outlined before, Arlandini *et al.* [2] have shown that the branchings at ^{151}Sm and ^{154}Eu are significantly better reproduced by this approach, yielding 88 and 95 % of the solar ^{152}Gd and ^{154}Gd abundance, respectively. Since the sensitivity of this test depends obviously on the quality of the nuclear physics part, a more reliable assessment of these data is indispensable in order to reach a conclusive situation.

VI. SUMMARY

The present attempt to improve the data basis for s-process studies in the important lanthanide region includes

TABLE X. Branching analyses using the classical approach.

Run	Parameters	^{148}Sm	$N_s/N_\odot$ (%) [a] ^{152}Gd	^{154}Gd	^{164}Er	Abundance pattern acceptable?
Pm and ^{151}Sm data: Ref. [11];						
Eu data: this work; all other data: Ref. [26].						
1	$n41t30e15$ [b]	101.5	72	88	72	no
2	$n41t30e10$	101.5	77	88	84	no
3	$n41t30e5$	101.6	82	88	96	no
4	$n41t30e6$	101.6	81	88	93	almost, except ^{154}Gd
5	$n41t29e5$	101.5	74	87	93	no
6	$n41t31e5$	101.9	90	90	98	no
7	$n35t30e6$	103.6	94	91	80	no
8	$n47t30e6$	99.6	71	86	72	no
9	$n44t30e6$	100.6	76	87	74	no
10	$n45t31e6$	100.5	82	88	74	no
Same set of cross sections, but Pm data adopted from Ref. [26]						
11	$n41t30e6$	100.5	82	88	74	no
12	$n30t30e6$	99.2	108	93	85	no
13	$n30t28e6$	99.1	88	90	82	no
14	$n30t27e4$	99.1	82	89	87	almost, except ^{154}Gd
Same set of cross sections, but ^{151}Sm adopted from Ref. [26] as well						
15	$n30t30e6$	99.2	74	92	85	no
Expected values for acceptable abundance pattern						
		100	82	98	94	
			$<12\%$	$<2\%$	$\sim 6\%$	*p* process
			$\sim 6\%$			Massive stars

[a]Uncertainties of $N_\odot$ are $<1.4\%$ for all listed isotopes, whereas the N_s contributions depend only on the listed parameters of the stellar plasma (the Sm and Gd cross sections being known to better than 2% [26]).
[b]($n_n = 4.1 \times 10^8$ cm^{-3}, $kT = 30$ keV, $n_e = 15 \times 10^{26}$ cm^{-3}).

cross section measurements on six Sm, Eu, and Er nuclei. With these results previous discrepancies among the Eu data could be resolved, while the important cross section of the *s*-only isotope ^{164}Er has been established with improved accuracy. The experiments were carried out by repeated activations with particular emphasis on the experimental study of the related systematic uncertainties.

As an important complement to the cross sections measurements, statistical model calculations were performed in order to determine the missing cross sections of the unstable branch point nuclei as well as the effect of thermally excited nuclear states. These calculations were concentrated on the sequence of Eu isotopes and were based on a local parameter set which was consistent with the known experimental information in this mass region. Additionally, a Hauser-Feshbach model based on global parameters was used for comparison and to determine stellar enhancement factors. The cross section trend with neutron number is well described by the present calculations, in contrast to earlier work based on global parameter sets [38,39]. Significant differences are also observed for the enhancement effect due to excited states. These problems as well as previous discrepancies for the calculated Pm cross sections [11,55] suggest that a consistent theoretical description of these crucial data over a wider mass range should be envisaged. Experimental efforts to determine the cross sections of some unstable nuclei will constitute an essential part of such a study.

The astrophysical analysis and interpretation of the investigated branchings of the *s*-process path was found to be rather ambiguous due to the presently remaining uncertainties in the theoretical data. Nevertheless, the fact that the canonical *s* process did not allow for a consistent description of the various branchings seems to support the analysis of Arlandini *et al.* [2], where this approach was questioned on the basis of the abundance pattern of the neutron magic nuclei with $N = 82$. However, a final conclusion on this point as well as on the performance of more complex stellar *s*-process models can only be made with improved nuclear physics data for the unstable branch point nuclei.

[1] N. Grevesse, A. Noels, and A. Sauval, in *Cosmic Abundances, Astronomical Society of the Pacific Conference Series*, edited by S. Holt and G. Sonneborn (BookCrafters, San Francisco, 1996), Vol. 99, pp. 117–126.

[2] C. Arlandini *et al.*, Astrophys. J. **525**, 886 (1999).

[3] E. Zinner, S. Amari, and R. Lewis, Astrophys. J. Lett. **382**, L47 (1991).

[4] S. Richter, U. Ott, and F. Begemann, in *Nuclei in the Cosmos*

'92, edited by F. Käppeler and K. Wisshak (Institute of Physics, Bristol, 1993), p. 127.

[5] S. Richter, U. Ott, and F. Begemann, in *Proceedings of the European Workshop on Heavy Element Nucleosynthesis*, edited by E. Somorjai and Z. Fülöp (Institute of Nuclear Research of the Hungarian Acadamy of Science, Debrecen, 1994), p. 44.

[6] K. Wisshak *et al.*, Phys. Rev. C **48**, 1401 (1993).

[7] K. Wisshak *et al.*, Phys. Rev. C **52**, 2762 (1995).

[8] K. Wisshak *et al.*, Phys. Rev. C **57**, 391 (1998).

[9] F. Voss *et al.*, Phys. Rev. C **59**, 1154 (1999).

[10] K. Wisshak *et al.*, Phys. Rev. C **61**, 065801 (2000).

[11] K. Toukan, K. Debus, F. Käppeler, and G. Reffo, Phys. Rev. C **51**, 1540 (1995).

[12] F. Käppeler, K. Toukan, M. Schumann, and A. Mengoni, Phys. Rev. C **53**, 1397 (1996).

[13] S. Jaag and F. Käppeler, Phys. Rev. C **51**, 3465 (1995).

[14] S. Jaag and F. Käppeler, Astrophys. J. **464**, 874 (1996).

[15] G. Reffo, in *Development of a Reference Input Parameter Library for Nuclear Model Calculations of Nuclear Data, Report No. INDC(NDS)-321*, edited by P. Oblŏzinský (IAEA, Vienna, 1994), data available from the IAEA via ftp.

[16] H. Beer and F. Käppeler, Phys. Rev. C **21**, 534 (1980).

[17] W. Ratynski and F. Käppeler, Phys. Rev. C **57**, 595 (1988).

[18] H. Stoll, Die stellaren (n,γ)-Querschnitte von ^{152,154}Sm und ^{151,153}Eu, thesis, University of Karlsruhe, 1993.

[19] J. Best, Technical Report No. FZKA 5824, Forschungszentrum Karlsruhe, 1996.

[20] I. Barnes *et al.*, Pure Appl. Chem. **63**, 991 (1991).

[21] P. De Bièvre and P. Taylor, Int. J. Mass Spectrom. Ion Phys. **123**, 149 (1993).

[22] J. De Laeter, K. Heumann, and K. Rosman, J. Phys. Chem. Ref. Data **20**, 1327 (1991).

[23] E. Storm and H. Israel, Nucl. Data, Sect. A **7**, 565 (1970).

[24] R. Macklin and P. Young, Nucl. Sci. Eng. **95**, 189 (1987).

[25] V. Kononov, B. Yurlov, E. Poletaev, and V. Timokhov, Yad. Fiz. **27**, 10 (1978).

[26] Z. Bao *et al.*, At. Data Nucl. Data Tables **76**, 70 (2000).

[27] R. Macklin and J. Gibbons, Astrophys. J. **149**, 577 (1967).

[28] M. Mizumoto and M. Sugimoto, Nucl. Instrum. Methods Phys. Res. A **282**, 324 (1989).

[29] S. Bednyakov, G. Bokhovko, G. Menturov, and K. Dietze, Sov. At. Energy **67**, 675 (1990).

[30] M. Bokhovko *et al.*, in *Nuclear Data for Science and Technology*, *Research Reports in Physics*, edited by S. Qaim (Springer, Berlin, 1992), p. 62.

[31] M. Moxon, D. Endacott, and J. Jolly, Ann. Nucl. Energy **3**, 399 (1976).

[32] V. Kononov *et al.*, Yad. Fiz. **26**, 947 (1977).

[33] M. Mizumoto *et al.*, J. Nucl. Sci. Technol. **16**, 711 (1979).

[34] H. Beer, G. Walter, and R. Macklin, in *Capture Gamma-ray Spectroscopy and Related Topics*, edited by S. Raman (AIP, New York, 1985), p. 778.

[35] M. Rayet (private communication).

[36] N. N. D. Files, technical report, available via telnet://bnlnd2.dne.bnl.gov (Brookhaven National Laboratory, 1996).

[37] V. Shorin, V. Kononov, and E. Poletaev, Yad. Fiz. **19**, 5 (1974).

[38] J. Holmes, S. Woosley, W. Fowler, and B. Zimmerman, At. Data Nucl. Data Tables **18**, 305 (1976).

[39] M. Harris, Astrophys. Space Sci. **77**, 357 (1981).

[40] G. Reffo, F. Fabbri, K. Wisshak, and F. Käppeler, Nucl. Sci. Eng. **80**, 630 (1982).

[41] R. Winters *et al.*, Astrophys. J. **300**, 41 (1986).

[42] G. Reffo (private communication).

[43] J. Mughabghab, in *Neutron Cross Sections* (Academic, New York, 1984), Vol. 1, Part B.

[44] B. Singh, J. Szücs, and M. Johns, Nucl. Data Sheets **55**, 185 (1988).

[45] L. Peker, Nucl. Data Sheets **58**, 93 (1989).

[46] M. Lee, Nucl. Data Sheets **60**, 419 (1990).

[47] R. Helmer, Nucl. Data Sheets **65**, 65 (1992).

[48] R. Helmer, Nucl. Data Sheets **69**, 507 (1993).

[49] C. Reich, Nucl. Data Sheets **71**, 709 (1994).

[50] F. Käppeler, S. Jaag, Z. Bao, and G. Reffo, Astrophys. J. **366**, 605 (1991).

[51] F. Fabbri and G. Reffo (private communication).

[52] V. Benzi, A. Saruis, and F. Fabbri, technical report, CNEN, 1963.

[53] Z. Bao and F. Käppeler, At. Data Nucl. Data Tables **36**, 411 (1987).

[54] P. Möller, J. R. Nix, W. D. Myers, and W. J. Swiatecki, At. Data Nucl. Data Tables **59**, 185 (1995).

[55] T. Rauscher and F.-K. Thielemann, At. Data Nucl. Data Tables **75**, 1 (2000).

[56] K. Takahashi and K. Yokoi, At. Data Nucl. Data Tables **36**, 375 (1987).

[57] E. Anders and N. Grevesse, Geochim. Cosmochim. Acta **53**, 197 (1989).

[58] H. Beer and R. Macklin, Astrophys. J. **331**, 1047 (1988).

[59] N. Prantzos, M. Hashimoto, M. Rayet, and M. Arnould, Astron. Astrophys. **238**, 455 (1990).

[60] W. Howard, B. Meyer, and S. Woosley, Astrophys. J. Lett. **373**, L5 (1991).

[61] M. Rayet *et al.*, Astron. Astrophys. **298**, 517 (1995).

[62] C. Raiteri *et al.*, Astrophys. J. **419**, 207 (1993).

[63] J. De Laeter (private communication).

[64] F. Käppeler, Prog. Part. Nucl. Phys. **43**, 419 (1999).

[65] M. Busso, R. Gallino, and G. Wasserburg, Annu. Rev. Astron. Astrophys. **37**, 239 (1999).

[66] E. Burbidge, G. Burbidge, W. Fowler, and F. Hoyle, Rev. Mod. Phys. **29**, 547 (1957).

[67] P. Seeger, W. Fowler, and D. Clayton, Astrophys. J., Suppl. **97**, 121 (1965).

[68] R. Ward, M. Newman, and D. Clayton, Astrophys. J., Suppl. **31**, 33 (1976).

[69] O. Straniero *et al.*, Astrophys. J. Lett. **440**, L85 (1995).

[70] R. Gallino *et al.*, Astrophys. J. **497**, 388 (1998).

[71] M. Lee, Nucl. Data Sheets **37**, 3 (1982).

[72] V. Shirley, Nucl. Data Sheets **43**, 127 (1984).

[73] R. Auble, Nucl. Data Sheets **40**, 301 (1983).

[74] P. Möller and R. Nix, At. Data Nucl. Data Tables **39**, 213 (1988).